Eur Radiol (2007) 17: 2780–2793
DOI 10.1007/s00330-007-0701-3

J. J. Nikken
G. P. Krestin

MRI of the kidney—state of the art

Received: 10 May 2006
Revised: 25 April 2007
Accepted: 10 May 2007
Published online: 24 July 2007

J. J. Nikken (✉) · G. P. Krestin
Department of Radiology, Erasmus MC, University Medical Center Rotterdam,
's Gravendijkwal 230,
3015 CE Rotterdam, The Netherlands
e-mail: j.nikken@erasmusmc.nl
Tel.: +31-10-4639222
Fax: +31-10-4634033

Abstract Ultrasound and computed tomography (CT) are modalities of first choice in renal imaging. Until now, magnetic resonance imaging (MRI) has mainly been used as a problem-solving technique. MRI has the advantage of superior soft-tissue contrast, which provides a powerful tool in the detection and characterization of renal lesions. The MRI features of common and less common renal lesions are discussed as well as the evaluation of the spread of malignant lesions and preoperative assessment. MR urography technique and applications are discussed as well as the role of MRI in the evaluation of potential kidney donors. Furthermore the advances in functional MRI of the kidney are highlighted.

Keywords Humans · Kidney diseases · Kidney neoplasms · Magnetic resonance imaging

Introduction

The role of computed tomography (CT) and magnetic resonance imaging (MRI) in the evaluation of renal abnormalities is ever increasing. Although multidetector helical CT has taken the largest leap, MRI can be used in case of compromised renal function, severe contrast allergy, or in case radiation exposure is a problem, such as in children and pregnant women. Furthermore, MRI can be used as a problem-solving modality when the CT findings are nondiagnostic. Attempts are being made to use MRI for imaging of renal function, including perfusion [1, 2], glomerular filtration rate [1, 3, 4] and intrarenal oxygen measurement [1, 5].

MRI technique

In MRI of the kidneys, fast imaging techniques are essential because of respiratory motion of the kidneys [6]. When possible the scan should be performed within one breath-hold. The patient should get clear instructions on breath-hold technique. If the patient has difficulty with breath-holding, a short period of hyperventilation before breath-holding may be helpful. The scan should be performed during expiration because the kidney position is more constant in expiration than in inspiration. If the sequence is too long to perform in one breath-hold, respiratory triggering can be used [6]. Another technique of respiratory motion control is respiratory gating by use of a navigator pulse. In this technique the movement of the diaphragm is monitored by a very fast 1D MRI sequence. If breath-holding is not possible, signal averaging can be used, but the quality of the images will be limited. The use of a phased array body coil is preferable because of the improved signal-to-noise ratio. To prevent aliasing in coronal imaging, the patient's arms should be raised above the head, or the arms may be supported by cushions, anterior to the coronal plane through the kidneys.

The imaging protocol for evaluation of the kidney at our institution on a 1.5-Tesla (T) MRI system consists of the following sequences:

1. Coronal T2-weighted half Fourier single-shot turbo spin echo sequence (HASTE) (TR infinite, TE 120 ms, flip angle 90°, breath-hold), serving as a localizer, but

also supplying valuable T2-weighted information. The limitation of this sequence is a relatively low signal-to-noise ratio.
2. Axial T2-weighted turbo spin echo sequence with fat suppression (TR 2,000 ms, TE 100 ms, flip angle 90°, respiratory triggering). This sequence provides for more detailed T2-weighted information. The T2-weighted sequence is especially helpful in characterizing cysts and intraparenchymal abscesses and in evaluating hydronephrosis. Furthermore, the T2-weighted sequence is helpful in detecting solid lesions.
3. Axial T1-weighted gradient echo sequence, in-phase and opposed-phase (TR 180 ms, TE 2.3 ms/4.6 ms, flip angle 90°, breath-hold), preferably as a dual-echo sequence. Many solid renal lesions are hypointense compared to the renal parenchyma on T1-weighted images, but lesions with hemorrhage, lesions with macroscopic fat, melanin-containing lesions and cysts with high protein content may show hyperintense signal [6]. Opposed-phase T1-weighted gradient echo sequences can be used to prove the presence of small amounts of fat.
4. Axial T1-weighted gradient echo sequence for dynamic imaging (TR 130 ms, TE 1.0 ms, flip angle 90°), using 30 ml intravenous gadolinium contrast, immediately followed by three breath-hold periods with four scan series per breath-hold. In this way pre-contrast and post-contrast images in arterial and nephrographic phase are obtained. Gadolinium-enhanced images are used for lesion detection and characterization.
5. Coronal 3D fast gradient echo with fat suppression, obtained immediately after the dynamic series for delayed contrast-enhanced images (TR 3 ms, TE 2 ms, flip angle 15°). This sequence can be used for renal venous anatomy, for the analysis of (tumor) thrombus and for evaluation of extent of the tumor in the perinephric fat.

Currently 1- to 1.5-T systems are generally used for abdominal imaging, but the advent of 3-T MRI systems brings a twofold increase in the signal-to-noise ratio (SNR). The increase in SNR can be spent on higher resolution or on even faster imaging. When combined with parallel imaging techniques such as sensitivity encoding (SENSE), the speed of any sequence can be increased by up to a factor of four or higher. However, although 3-T MRI is promising, only a limited amount of research has been published on 3-T MR imaging for renal lesions, and its value has still to be established [7, 8].

Renal lesions

The main goal in the evaluation of renal lesions is to differentiate surgical lesions from nonsurgical lesions. Most simple cysts are easily recognized and don't need further analysis. Complicated or multiloculated cysts need more attention in order to differentiate them from cystic carcinomas. In most solid renal lesions, neither CT nor MRI is able to reliably distinguish benign from malignant. Some solid lesions, however, may be identified as benign with high confidence, like angiomyolipomas. In general, if a lesion cannot be characterized as benign or malignant, it should be considered malignant [9].

Malignant renal lesions

Renal cell carcinomas

Renal cell carcinomas account for 3% of all malignancies in adults. Almost 50% are detected incidentally. As many as 85% of suspicious renal lesions are malignant [10]. Features indicating potential malignancy of a renal lesion are size of the lesion, the presence of calcifications, the distribution of the calcifications within the lesion, wall thickness and the presence of septa in case of a cystic lesion (Fig. 1), inhomogeneity of the lesion, extension of the tumor beyond Gerota's fascia, and last but not least, enhancement after contrast administration. Concerning calcifications in cystic lesions, recent research suggests that the importance of these calcifications as a determinant of malignancy is relatively low [11].

Duchene found in 186 renal tumors that all tumors greater than 7 cm (n=48) were malignant. About 80% of tumors smaller than 3 cm were malignant [10]. The differential diagnosis of solid renal lesions smaller than 7 cm consists of oncocytoma, angiomyolipoma, hemangioma, leiomyoma, and focal xanthogranulomatous pyelonephritis. Of these lesions, only cysts and angiomyolipomas can often be positively identified as benign lesions.

Generally, MRI is performed only after a renal lesion has been detected by ultrasound or CT. CT may be followed by MRI if the enhancement at CT imaging is indeterminate (10–20 Hounsfield Units) [12] or in case of suspected pseudo-enhancement. At CT examination, simple cysts may show pseudo-enhancement after intravenous contrast administration, which is an increase in attenuation of more than 10 Hounsfield Units, not caused by administered contrast or by partial volume effect but by technical factors [13].

Assessment of enhancement

The main MRI feature indicating potential malignancy of a renal tumor is enhancement after intravenous gadolinium administration, differentiating the lesion from a cyst. However, enhancement at MRI cannot be measured as easily as enhancement at CT. The MR signal is not calibrated, in contrast to density at CT imaging. The MRI signal depends not only on tissue characteristics, but also on the size of the patient, the gain setting of the MR system, the pulse sequence

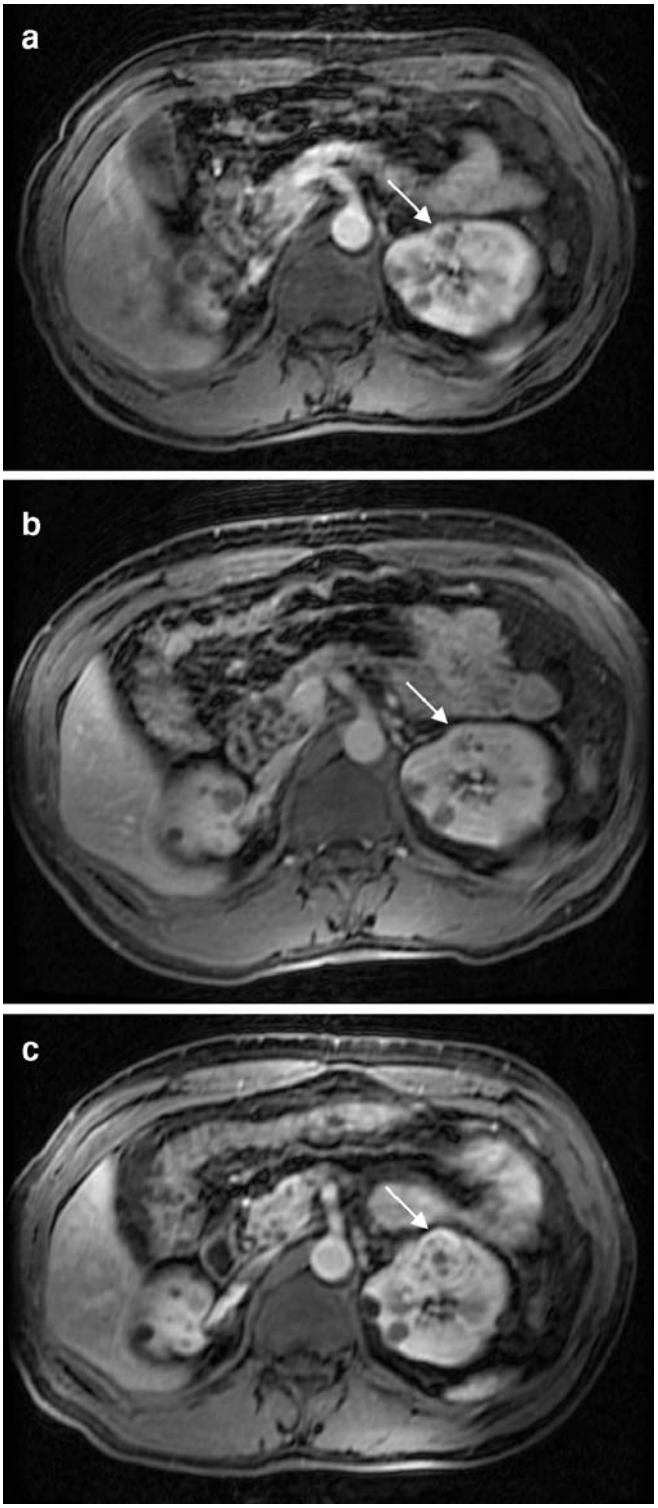

Fig. 1 Gradient echo images with intravenous gadolinium at baseline (**a**), 8 months later (**b**) and 15 months later (**c**). The complicated cortical cyst (*arrow*) in the left kidney on image (**a**) in a patient with Von Hippel Lindau disease progresses into a frank renal cell carcinoma with multiple enhancing internal septations (**c**). Several simple cysts are visible. Images courtesy of Roy S. Dwarkasing

and the coils. The presence of enhancement can be assessed subjectively, by subtraction imaging, and by quantitative assessment. Subjective assessment of enhancement has been shown to be accurate in detecting renal cell carcinomas [14]. However, in a cystic lesion with only a small solid component, subjective assessment may be difficult and subtraction images may be used to better assess the presence of enhancement. It is important to realize that renal cell carcinomas may be hypovascular and therefore may show less enhancement than the surrounding renal parenchyma [15]. Also in these hypovascular lesions and in lesions that are hyperintense on T1-weighted imaging, subjective assessment may be difficult, and subtraction images may be of particular use [16].

Some investigators have studied quantitative assessment of enhancement by calculating the relative enhancement defined as the signal intensity increase after contrast administration compared to the signal intensity before contrast administration. Ho used relative signal intensity enhancement to differentiate cysts from malignant lesions. Using a threshold of 15% relative signal intensity enhancement after administration of intravenous gadolinium, Ho found in 74 patients with renal lesions a sensitivity of 100% and a specificity of 94% in the detection of renal cell carcinomas [17]. The relative enhancement peak was maximum between 2 and 4 min after injection of gadolinium contrast. It is worthwhile to note that cysts also showed a mean enhancement change of up to 5%. This pseudo-enhancement may be attributed to motion artifacts and volume averaging [14].

Subtypes of renal cell carcinoma

Several histological subtypes of renal cell carcinoma are recognized. The most frequent subtype is the conventional or clear cell carcinoma, which comprises 88% of all renal cell carcinomas, followed by papillary carcinoma (10%) and chromophobe carcinoma (2%). Collecting-duct carcinoma is very rare. The first three subtypes do not differ significantly in prognosis and show a 5-year survival rate of 73–88% [18]. Several attempts have been made to distinguish the subtypes of renal cell carcinoma by imaging features using CT characteristics [19, 20]. There are only a few studies using MRI to differentiate the subtypes of renal cell carcinoma. Outwater et al. described that clear cell carcinomas may show loss of signal intensity on opposed-phase images compared to in-phase images, due to intracellular lipid [21]. This effect is caused by the presence of fat and water protons in the same voxel, resulting in cancellation of the signal on the opposed-phased sequence. The intracellular lipid contributes to the histological appearance of the clear cell. Because oncocytoma and transitional cell carcinoma do not contain diffuse lipid, the loss of signal on opposed-phase images may allow differentiation between clear cell carcinoma on the

one hand and oncocytoma and transitional cell carcinoma on the other hand. However, this distinction is of little clinical use. If the tumor does not show signal loss, it can still be a clear cell carcinoma [21].

Fat-containing renal cell carcinomas

Although rare, it has been claimed that renal cell carcinomas may contain macroscopic fat. Since intralesional fat has long been considered diagnostic for angiomyolipoma, these rare fat-containing renal cell carcinomas may easily be confused with angiomyolipoma. A few cases of fat-containing renal lesions, suggestive of angiomyolipoma, that appeared to be renal cell carcinoma have been reported [22–27]. With a few exceptions [25, 27], most of the reported cases also contained intratumoral calcifications [22–26], which is very rare in angiomyolipoma. Therefore, the presence of calcification in a lesion with macroscopic fat should be a warning that the lesion may very well be a carcinoma [28]. Because the accuracy of MRI in detecting calcifications is relatively low, it is important always to assess earlier ultrasound or CT examinations of the patient, which will likely have been made in most cases.

Less than 5% of renal cell carcinomas are cystic [9] (Fig. 2). On CT imaging, cystic renal lesions are classified using the Bosniak classification system [29]. This system was developed for CT, but recently its use has been evaluated in MRI by Israel et al. [12]. The CT and MRI findings in this study were similar in 81% of 69 renal masses. In the remaining 19% of cases, MRI showed more septa, increased wall thickness or increased enhancement compared to CT. This resulted in an upgrade of the Bosniak classification in seven cases (10%), of which two cases were upgraded to category 3 and two cases to category 4. The latter two cases appeared to be malignant at surgery. One of the cases upgraded to category 3 appeared to be benign, and the second one showed progression (patient refused surgery). The authors state that the Bosniak grading system is appropriate for use in MRI, but acknowledge that further research is necessary [12].

Staging

There are two staging systems for renal cell carcinoma, both based on the degree of tumor spread beyond the kidney. The Robson staging system [30] (Table 1) is still in use, but it is being replaced by the TNM staging system, developed by the American Joint Committee on Cancer (AJCC) [31] (Table 2). The TNM staging system is similar to the Robson system, but provides a more detailed description. Staging is usually performed using CT. Hallscheidt compared the performance of CT and MRI in the TNM system and found a similar accuracy in the staging of renal cell carcinoma [32].

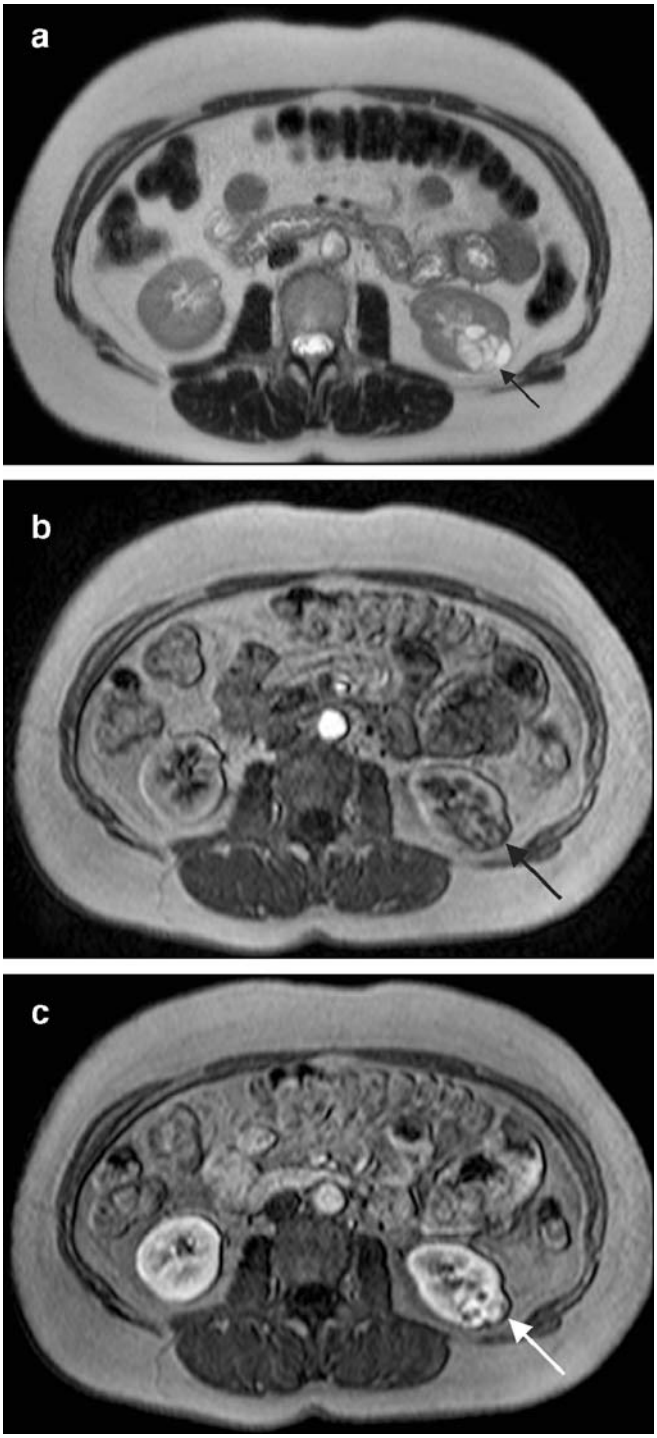

Fig. 2 T2-weighted turbo spin echo sequence (**a**) showing a cystic multiloculated lesion in the left kidney (*arrow*) with high signal intensity content. The pre- and post-gadolinium images (**b** and **c**) show enhancement of the septations. Pathologic examination showed a cystic renal cell carcinoma

Table 1 Robson staging system for renal cell carcinoma [30]

Stage	Tumor extent
I	Tumor confined to the kidney
II	Tumor extension through the capsule of the kidney in the perirenal fat including the adrenal gland, no involvement of Gerota's fascia
IIIa	Tumor extension into the renal vein or inferior vena cava
IIIb	Involvement of regional lymph node(s)
IIIc	Involvement of regional lymph node(s) and extension into the renal vein or inferior vena cava
IVa	Tumor extension beyond Gerota's fascia into adjacent organs
IVb	Distant metastasis

Determination of the extent of the tumor into the renal vein and the inferior vena cava (IVC) (TNM stage T3b and T3c) is important for the surgical approach. Involvement of the IVC is reported to occur in 4–10% of renal cell carcinoma patients [33]. If the tumor extends into the large veins, the upper level of the tumor thrombus dictates the surgical approach. If the extension is limited to the renal vein, it is necessary to know the distance to the IVC, in order not to dissect the renal vein through the intraluminal tumor. Extension into the IVC requires cavotomy with clamping of the IVC and the contralateral renal vein (Fig. 3). If a tumor thrombus extends above the hepatic veins, the liver should be mobilized to control the IVC above the hepatic veins. Extension into the right atrium generally requires cardiopulmonary bypass during surgery with hypothermic cardiac arrest [33].

For differentiation between bland thrombus and tumor thrombus, the use of gadolinium contrast is indicated, since the enhancement of the thrombus indicates a tumor, whereas the lack of enhancement indicates a clot [34]. Before the introduction of multidetector CT scanners, MRI was considered to be superior to CT in the assessment of intravenous tumor extension, especially at the level of the intrahepatic IVC. However, multislice helical CT scanners are nowadays able to generate multiplanar reconstructions in any direction at high resolution. Recent studies

Table 2 AJCC TNM staging system for renal cell carcinoma (2002, sixth edition) [31]

Stage	Description
Tx	No information on primary tumor available
T0	No evidence of primary tumor
T1a	Tumor size 4 cm or less, limited to the kidney
T1b	Tumor size more than 4 cm but no more than 7 cm, limited to the kidney
T2	Tumor size more than 7 cm, limited to the kidney
T3a	Tumor extension into the perinephric fat and/or renal sinus fat or the adrenal gland, but not beyond Gerota's fascia
T3b	Tumor grossly extends into the renal vein or its segmental (muscle-containing) branches, or inferior vena cava below the diaphragm
T3c	Tumor grossly extends into the inferior vena cava above the diaphragm or invasion of the IVC wall
T4	Tumor extension beyond Gerota's fascia
Nx	No information on regional lymph nodes available
N0	No regional lymph node metastasis
N1	Metastasis in a single regional lymph node
N2	Metastasis in more than one regional lymph node
Mx	No information on distant metastases available
M0	No distant metastases
M1	Distant metastases

Fig. 3 T1-weighted gradient echo sequence after intravenous contrast of a large renal cell carcinoma in the upper pole of the left kidney with tumor thrombus extending into the IVC up to the level of the liver

comparing multidetector CT (MDCT) and MRI showed no difference in accuracy of MDCT and MRI in assessing the extension of thrombus in the IVC [35, 36].

Invasion of the IVC wall (TNM stage T3c) is important to detect because in that case the surgeon has to partially resect and reconstruct the IVC. The accuracy of MRI in IVC wall invasion has not yet been well documented. One study reported a sensitivity of 100% and a specificity of 89% in the detection of IVC wall involvement, however, this study consisted of only 12 patients and no inclusion criteria were reported [33]. In this study it was noted that altered signal in the vessel wall and wall enhancement were nonspecific. The most reliable sign of IVC wall invasion was tumor signal both inside and outside the vessel wall [33].

The detection of lymph node metastasis by CT mainly relies on the size of the lymph nodes. In recent years, several studies have been published on the use of ultrasmall superparamagnetic iron oxide particles (USPIO) as a negative contrast agent for the detection of small lymph node metastasis. The USPIO particles consist of an iron-oxide core covered with a low-molecular-weight dextran coating. After intravenous injection, the USPIO particles accumulate in healthy lymph nodes. The USPIOs are ingested by macrophages through phagocytosis and cause a decrease in signal intensity on T2- and T2*-weighted images. Gradient echo sequences are the most sensitive for these susceptibility effects. Lymph node metastases displace the macrophages in the lymph node and therefore do not show the loss in signal intensity seen in normal lymph nodes. To our knowledge no studies have been published on the use of USPIOs in renal cell carcinoma. However, a recent meta-analysis by Will et al. [37] describes the pooled results of several studies on USPIOs for several types of metastasis. In these studies, MRI with and without ferumoxtran, a first-generation USPIO, was compared with histology. MRI with ferumoxtran significantly improved the diagnostic precision compared to MRI without ferumoxtran. It was shown to be both sensitive and specific, especially in the detection of abdominal and pelvic metastasis.

MRI in nephron-sparing surgery

In recent years, interest in nephron-sparing surgery has been growing. At first, partial nephrectomy was mainly performed in case of a solitary kidney or diminished renal function, in order to preserve as much function as possible. Due to improving techniques and to increasing application of modern imaging modalities, the number of small, incidentally detected renal tumors is increasing [38]. This development has encouraged surgeons to use nephron-sparing surgery also for patients with normal renal function. The long-term follow-up data suggest that survival after partial nephrectomy of small renal cell carcinomas is comparable to total nephrectomy [39]. The ideal tumor for partial nephrectomy is smaller than 3 cm, is confined to the parenchyma of the kidney and has a peripheral location [40]. The presence of a pseudocapsule around a renal tumor is a sign of lack of perinephric fat invasion and therefore a favorable sign for partial nephrectomy [38, 41]. A pseudocapsule consists of compressed renal tissue and fibrous tissue. The sensitivity of CT in depicting a pseudocapsule is low (10–26%), whereas MRI shows a moderate to high sensitivity in depicting the pseudocapsule (54–93%) [41, 42]. On MRI, a pseudocapsule presents as a hypointense rim around the tumor on both T1-weighted and T2-weighted images, but can be best seen on the T2-weighted images and sometimes on gadolinium-enhanced GRE images [40].

Transitional cell carcinoma

Transitional cell carcinoma of the kidney is usually evaluated by intravenous urography, CT and endoscopy. However, MRI may play a role if CT and endoscopy are not feasible. CT may not be possible in case of poor renal function, and in case of ureteral obstruction, contrast excretion may be too limited to allow tumor detection. The ureter may not be accessible for endoscopy because of fibrosis and stricture of the ureter and ureter ostium. This may especially be the case in patients who have been treated for bladder cancer. These patients are at particularly increased risk for upper urinary tract transitional cell carcinoma [43]. Transitional cell carcinoma of the pyelum or ureter will

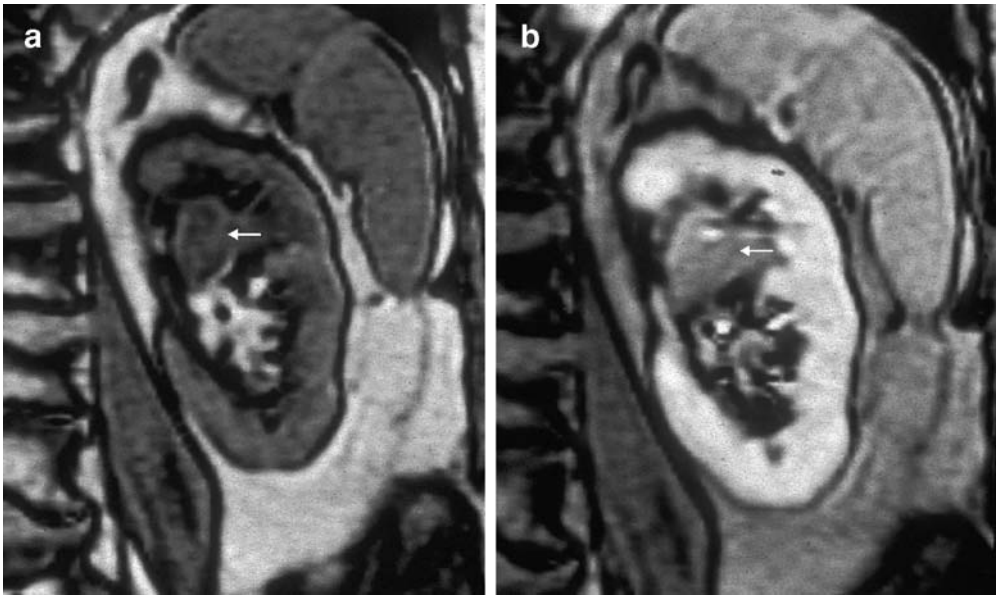

Fig. 4 T1-weighted gradient echo images before (**a**) and after (**b**) gadolinium administration. A mass in the renal pelvis (*arrow*) shows moderate enhancement after gadolinium administration. A transitional cell carcinoma was suspected, which was confirmed after nephrectomy

generally show as an irregular mass projecting in the lumen. In the collecting system, transitional cell carcinoma is usually confined to the lumen (Fig. 4), but infiltrative growth into the renal parenchyma occurs and typically does not distort the renal contour. Chahal et al. applied MR urography (MRU) in 23 patients with high clinical suspicion of upper tract transitional carcinoma and hydronephrosis that could not be explained with other imaging modalities. MRU showed five renal pelvic transitional cell carcinomas and eight ureteral transitional cell carcinomas, confirmed by histology. In the remaining patients, no sign of transitional cell carcinoma was observed during 1-year follow-up [43]. Although these results are promising, the number of publications on MRI for transitional cell carcinoma is limited and more research is required to determine the value of MRI for the detection of transitional cell carcinoma.

Benign renal lesions

Oncocytoma

Oncocytomas are benign, most often asymptomatic renal tumors. They represent 2–12% of renal masses. On MRI,

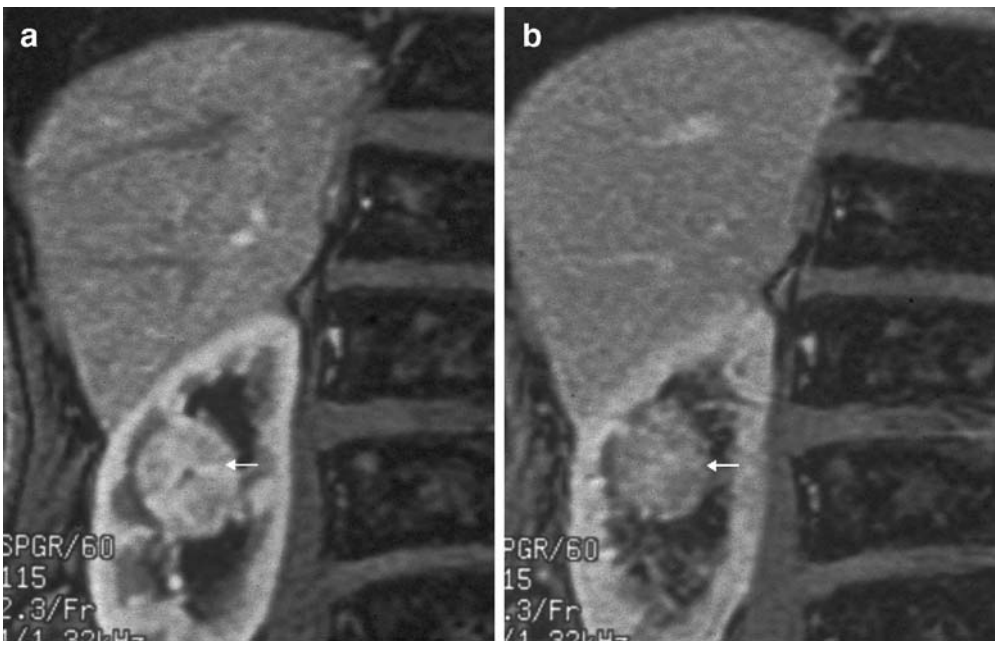

Fig. 5 Post-contrast fat-suppressed T1-weighted gradient echo images, arterial phase (**a**) and nephrographic phase (**b**) of a central oncocytoma (*arrow*). The tumor shows a hypointense central scar in the arterial phase. In the nephrographic phase, the central scar is slightly hyperintense

oncocytomas show variable low signal intensity on T1-weighted images (Fig. 5) and heterogeneous high signal intensity on T2-weighted images. In 33–54% a central scar with low signal intensity on both T1- and T2-weighted images is visible. After contrast enhancement a spoke-wheel-like pattern may be observed [44]. Both a central scar and spoke-wheel pattern, however, may also be seen in renal cell carcinomas [38, 45] and are therefore not specific for oncocytomas. Oncocytomas may show a pseudocapsule, consisting of compressed renal parenchyma and fibrous tissue. One should be aware that a pseudocapsule is not specific for oncocytoma, since renal cell carcinomas can also be surrounded by a pseudocapsule. Because the characteristics of oncocytomas show considerable overlap with the characteristics of renal cell carcinomas, the therapy for a suspected oncocytoma is usually surgical [38].

Angiomyolipoma

Angiomyolipomas are benign hamartomatous tumors, consisting of fat, smooth muscle and blood vessels. Angiomyolipomas are the only solid renal tumors that can be positively characterized using MRI [46]. Angiomyolipomas are identified by demonstrating macroscopic fat in the lesion (Fig. 6). The ability to differentiate angiomyolipomas is especially urgent in patients with tuberous sclerosis, since angiomyolipomas develop in about 80% of these patients, and at the same time these patients are at an increased risk of developing renal cell carcinomas. Macroscopic fat in a renal lesion can be detected by CT using density measurement and by MRI using fat-suppression techniques. On the opposed-phase gradient echo images, macroscopic fat is demonstrated by a hypointense rim surrounding the fat (India ink artifact)

Fig. 6 T1-weighted gradient echo image (**a**), post-contrast fat-suppressed T1-weighted gradient echo image (**b**), and T2-weighted HASTE (half Fourier single-shot turbo spin echo) image of the left kidney (**c**). The hyperintense parts of the tumor in the lower pole (*black arrow*) on the T1-weighted image show a drop in signal intensity on the post-contrast fat-suppressed T1-weighted image, proving the presence of fat, while the hypointense parts of the tumor enhance after gadolinium. The fatty portions are hyperintense on the T2-weighted sequence, but not as high as the cyst (*white arrow*) in the midportion of the kidney. The MRI characteristics of the tumor in the lower pole are consistent with angiomyolipoma

[46]. It must be noted that the India ink artifact also occurs at the interface between tumors that don't contain fat and the surrounding perinephric fat, if the tumor extends into the perinephric fat.

If the amount of intralesional fat is small, the differentiation between angiomyolipoma and renal cell carcinoma may be difficult (Fig. 7). Kim et al. showed for CT that homogeneous enhancement and a prolonged enhancement pattern were significantly more prevalent in angiomyolipoma with minimal fat than in renal cell carcinoma [47]. Using both CT findings as a criterion for the differentiation of angiomyolipoma with minimal fat from renal cell carcinoma, they found a positive predictive value of 91% and a negative predictive value of 87%. It is likely that this is also the case in contrast-enhanced MRI, however this has not yet been proved.

It has been shown that clear cell carcinomas may show signal loss on opposed-phase images compared to in-phase images, due to intracellular lipid [21]. This loss of signal intensity should be distinguished from the signal loss at the interface of macroscopic fat and surrounding tissue in angomyolipomas on opposed-phase images, especially if the amount of macroscopic fat is small. If in doubt, the in-phase gradient echo images are often helpful because the fatty portion of angiomyolipomas will be hyperintense, whereas renal clear cell carcinomas are generally hypo- or isointense [6, 46]. Unfortunately, clear cell carcinomas are incidentally hyperintense on T1-weighted images [48]. In these cases spectral fat-suppression images should be used to prove the presence of macroscopic fat in the angiomyolipoma.

Attention should be paid to the possibility that carcinomas sometimes contain hemorrhage, causing high signal intensity on in-phase T1-weighted images. In these cases, opposed-phase images and spectral fat suppression will not show a drop in signal intensity.

Xanthogranulomatous pyelonephritis

Xanthogranulomatous pyelonephritis is a rare chronic pyelonephritis, which may result in severe renal impairment. It is most common in middle-aged women, but it may also occur in children. Often *Proteus* or *E. coli* species are involved and the pyelonephritis is often accompanied by calculi, most typically staghorn calculi. It may be accompanied by calyx obstruction and parenchymal abscesses. In xanthogranulomatous pyelonephritis, the affected renal parenchyma is replaced by lipid-laden macrophages, resulting in the typical yellow-gray appearance of the lesion at macroscopy. It may involve the whole kidney, or it may be focal. Especially when it is focal, xanthogranulomatous pyelonephritis may be mistaken for a renal carcinoma. On T1-weighted images, the solid component of the lesion may be isointense or hyperintense, which can be attributed to the fatty component. On T2-weighted images, the signal intensity of the solid component is isointense to slightly hypointense. The parenchymal cavities filled with fluid and pus show high signal intensity on T2-weighted images and low signal intensity in T1-weighted images, varying according to the protein con-

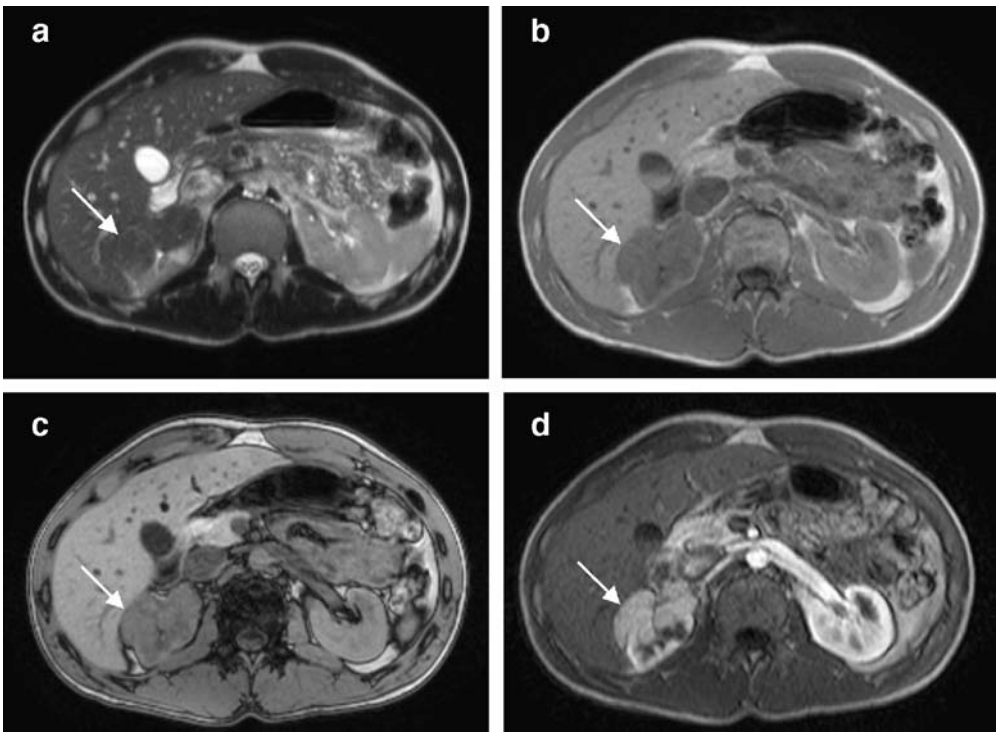

Fig. 7 Lesion in the upper pole of the right kidney in a patient with tuberous sclerosis (*arrow*). The lesion shows low signal intensity on T2-weighted turbo spin echo images (**a**) and intermediate signal intensity on in-phase T1-weighted gradient echo images (**b**). No signal loss is observed on the out-of-phase T1-weighted gradient sequence (**c**). The lesion shows moderate enhancement after intravenous gadolinium administration (**d**). Pathologic examination after resection of the lesion showed an angiomyolipoma. In this unusual case, no macroscopic fat was detected on MRI

centration in the cavity [49, 50]. In xanthogranulomatous pyelonephritis, the perirenal fascia may be thickened and show enhancement after gadolinium administration [49]. The absence of hyperintense signal on T2-weighted images of the solid components may be helpful in the differentiation between xanthogranulomatous pyelonephritis and renal tumor [50].

MR urography

In MR urography, the pyelocalyceal system and the ureters are visualized using heavily T2-weighted images or T1-weighted images with gadolinium contrast. On the heavily T2-weighted images, the urine in the pyelocalyceal system and ureters is hyperintense because of its long T2 relaxation time, whereas the surrounding tissue is hypointense. The HASTE or single-shot fast spin echo (SSFSE) is very suitable for this purpose; they are very fast with sufficient in-plane resolution [51]. The thin sections can be used for detailed evaluation; a maximum intensity projection is useful for overview of the urinary tract. For T2-weighted MR urography, it is essential that the urinary tract is sufficiently filled with urine. Therefore it is often necessary to use a diuretic if the urinary tract is not dilated [51]. Hagspiel et al. evaluated whether MRI of the urinary system of potential renal donors was feasible without diuretic stimulation or compression and found sufficient visualization of the urinary collecting system in only 14% of the rapid acquisition with relaxation enhancement (RARE) urograms and in 26% of the gadolinium-enhanced 3D fast low-angle shot (FLASH) urograms [52].

In contrast-enhanced MR urography, intravenous gadolinium can be combined with a T1-weighted 3D gradient echo sequence. In case the patient is unable to hold his breath, a fast 3D GRE EPI sequence can be used that offers the additional advantage of reduced ghost artifacts caused by ureteral peristalsis [53]. However, the conventional GRE images provide better high resolution images compared to the EPI images [53]. In contrast-enhanced MR urography, the images are acquired in the excretory phase, typically 5–8 min after intravenous gadolinium injection [51]. Additional use of a diuretic is advisable to increase excretion and to dilute the excreted contrast: if the excreted gadolinium is too concentrated, the T2* effect may cause signal loss [51]. The accuracy of MR urography in assessing renal obstruction is similar to CT urography [54, 55]. MRI has the advantage that it is better able to detect perirenal edema as a secondary sign of obstruction [54]. In a study by Sudah et al., gadolinium-enhanced MR urography showed renal calculi with considerably higher sensitivity than T2-weighted MR urography [55]. On MR urography, a calculus appears as a signal void, which is nonspecific: blood clots, gas, sloughed papilla and tumors may also appear as a low signal within the bright signal of urine [51]. If a signal void is not clearly detached from the wall of the pelvis or ureter, additional T1-weighted and contrast-enhanced images are necessary to further characterize the lesion.

MRI of potential donor kidneys

Due to the increasing demand for donor kidneys and the relative shortage of cadaver kidneys, the importance of living donors is increasing. Nephrectomy is increasingly performed by laparoscopic surgery to keep the burden for the donor as low as possible. A thorough pre-operative evaluation of the donor kidney is essential to keep the risks as low as possible. Especially for endoscopic nephrectomy, it is important for the surgeon to be informed about the arterial and venous vasculature of the kidney, about the presence of accessory vessels and about abnormal vessel location, like extrahilar branching and retrocaval position of vessels. Moreover, the surgeon needs to be informed about the presence of an abnormal collecting system and the presence of cysts or tumors [56].

In the imaging protocol, special attention should be focused on arterial and venous imaging, in addition to the standard parenchymal imaging. For the arterial MR angiography, a 3D fast GRE with intravenous gadolinium after timing bolus can be used (TR 4.7 ms, TE 1.4 ms, flip angle 30°), with coronal thin-section reconstructions. A relatively large flip angle (up to 40°) can be used to minimize background signal around the high signal of the renal arteries [56]. The venous angiography sequence should follow the arterial angiography immediately. Due to the excretion of gadolinium by the kidneys, the concentration of gadolinium in the renal veins is lower than in the renal arteries, causing lower contrast of the veins compared to the background. A lower flip angle (15°) can be used to compensate for the lower gadolinium concentration, at the expense of more background signal [56]. The 3D dataset can be used for the reconstruction of thin 2D sections for detailed evaluation, as well as for maximum intensity projection (MIP) reconstructions of the vessels (Fig. 8).

Although the time–of-flight technique can be used to evaluate renal arteries, it is not recommended for the detection of accessory renal arteries of small caliber [57]. It may be used to clarify intraluminal filling defects potentially caused by flow artifacts on gadolinium-enhanced MR angiography [6]. Phase contrast imaging can be used for detection and grading of renal artery stenosis [58, 59] but has limitations in evaluating potential kidney donors. The problem of motion artifacts in phase contrast imaging caused by the long acquisition time can be overcome by using interleaved gradient echo-planar technique, shortening the acquisition time from minutes to about 30 s [59]. However, it is difficult to select the proper velocity encoding gradient [6], and tortuous venous anatomy and low flow limit the use of phase contrast MRI in potential kidney donors [56].

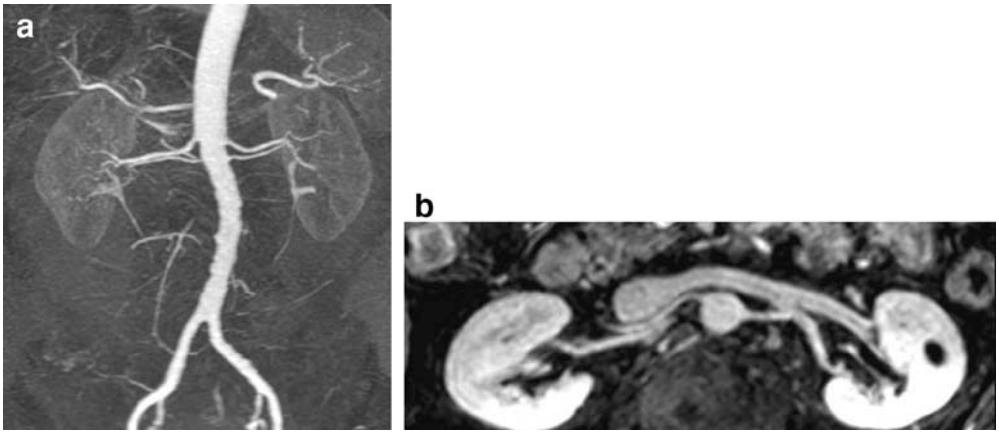

Fig. 8 Pre-operative imaging of potential donor kidneys. **a** Gradient echo image after intravenous contrast, arterial phase, TR 3 ms, TE 1 ms, slice thickness 2.2 mm, flip angle 27°, coronal. **b** Gradient echo image after intravenous contrast, nephrographic phase, TR 4 ms, TE 1 ms, slice thickness 2.2 mm, flip angle 15°, coronal. The lower flip angle in the depiction of the renal veins was chosen to compensate for the lower gadolinium concentration in the renal veins

Most studies on the accuracy of MR angiography (MRA) in the evaluation of renal vessels compared to digital subtraction angiography and CT angiography show similar or even better results [60–63], although not all studies confirm these findings [64]. In a recent study on 111 MRA examinations for donor nephrectomy, nine accessory arteries were missed, requiring anastomosis in four arteries. Of 14 kidneys with more than one vein, only 4 were identified by MRA, requiring anastomosis in 1 case [65].

MRI for imaging of renal function

In recent years, progress has been made in the use of MRI for the evaluation of renal function. Renal disease often causes impairment of renal function. Measurement of renal function can be used as an indicator of severity of disease and can direct therapy. The most simple tests of renal function are serum creatinine and creatinine clearance. However, these tests do not provide information about the function of each individual kidney. This information can be important in case of a living renal kidney donor, prior to nephrectomy or in case of renal artery stenosis. Renal scintigraphy provides information about the function of each kidney, but this test lacks anatomic detail. CT has the disadvantage of ionizing radiation and the use of potentially nephrotoxic contrast, which generally isn't a problem in healthy kidneys, but may cause deterioration of renal function in diseased kidneys. MRI has the potential to combine the functional and anatomic information about each kidney individually [66].

Perfusion

Measurement of renal perfusion may be a tool to assess the significance of renal artery stenosis and to assess ischemic nephropathy, and it may be used in renal transplant assessment. Several techniques have been studied to measure renal perfusion [1]. The maximum slope Gd-DTPA technique uses the maximum slope of the Gd-DTPA enhancement curve in relation to the maximum Gd-DTPA concentration in the aorta to calculate renal blood flow. The Gd-DTPA concentration in the aorta can be calculated using pre-contrast and post-contrast relaxation times measured in the aorta, assuming a linear relationship between gadolinium concentration and the inverse of the pre- and post-contrast T1 difference. Calibration of the signal intensity is performed using phantoms with increasing gadolinium concentration [67].

Furthermore, attempts have been made to assess renal perfusion by arterial spin labeling. To prevent leakage of the contrast medium into the extravascular space, albumin-bound contrast agent is used [68]. However, the different MRI renal perfusion techniques still need to be validated so more research is needed to assess the clinical usefulness.

Glomerular filtration rate

The glomerular filtration rate (GFR) is a parameter that is used to assess renal function. The serum creatinine level is a rough indicator of the glomerular filtration rate, it is easy and cheap to obtain, but it provides no information about each individual kidney. For the measurement of the GFR by MRI, several techniques have been investigated. The first technique used MR spectroscopy to measure the T1 relaxation times of urine and serum samples taken at intervals after intravenous gadolinium administration. Calculation of the glomerular filtration rate was based on the linear relationship of 1/T1 to the serial dilution measurements of the serum and urine samples [69]. This technique still had the disadvantage of measuring the GFR of both kidneys together.

Another MR technique assessing each individual kidney was developed by calculating the extraction fraction (EF) of Gd-DTPA, which is the difference between renal arterial and renal venous Gd-DTPA concentration, normalized to the arterial Gd-DTPA concentration: $EF = (Gd^{art} - Gd^{venous})/Gd^{art}$. The gadolinium concentrations can be calculated after measurement of the T1 relaxation time of arterial and venous blood before and after intravenous gadolinium administration,

using the formula $1/T1^{post} = 1/T1^{pre} + [Gd]*R$, where R is the relaxivity of gadolinium, and $T1^{pre}$ and $T1^{post}$ are the T1 relaxation times before and after intravenous gadolinium. The glomerular filtration rate can then be calculated according to the formula $GFR = EF * RBF * (1 - Hct)$, where RBF is renal blood flow, which can be measured by phase contrast flow quantification [3], and Hct is hematocrit [66].

An alternative MRI technique to measure glomerular filtration rate also uses contrast-enhanced dynamic MRI and is based on a the time-dependent concentrations of Gd-DTPA in the cortex and the medulla—a two compartment model [1]. The different techniques to measure glomerular filtration rate still need to be validated, and their role in clinical practice needs to be established.

Diffusion-weighted MRI

In diffusion-weighted MR imaging, the image contrast is influenced by the Brownian motion of water molecules. The signal intensity is high if water molecules are restricted in their motion, which can be caused by cell membranes or, in the case of free fluid, by high viscosity. The MR signal intensity is low if water molecules can diffuse freely. Diffusion-weighted imaging has found its place in neuroradiology, especially for the early detection of ischemic brain lesions. Diffusion MRI can also be used for fiber tract mapping in cerebral white matter, by measuring the directional components of the diffusion. Because diffusion-weighted images are inherently T2-weighted, the images are influenced by the T2-shine-through effect. This is the presence of high signal intensity in restricted water, caused by the T2 effect. To cope with this effect, the apparent diffusion coefficient (ADC) may be calculated from two images acquired with different gradient duration and amplitude (b-values) and used for ADC mapping.

In renal MR imaging, the role of diffusion MRI is not yet as clear as in neuro-imaging. Fukuda et al. showed that diffusion in the kidney is anisotropic, due to the radial orientation of the tubules in the pyramids and the blood vessels in the renal cortex [70] (Fig. 9). Diffusion-weighted MRI has been applied in patients with solid renal masses as well as in pyelonephritis and renal failure [71, 72]. ADC mapping showed differences between the lesions and normal tissue, but more research is needed to know whether diffusion-weighted MRI can actually help in characterizing different abnormalities. Diffusion-weighted imaging has been applied to differentiate between hydronephrosis and pyonephrosis. Chan et al. found in a limited group of patients that diffusion-weighted imaging showed a hypointense pyelocalyceal system in hydronephrosis and a hyperintense pyelocalyceal system in pyonephrosis [73]. The hyperintensity in pyonephrosis is thought to be due to the high viscosity of the pus, whereas the free-moving molecules in hydronephrosis cause low signal intensity. The results of diffusion-weighted MRI in the kidney are still preliminary, and more research should reveal the value of its clinical application.

Fig. 9 Diffusion-weighted tensor image of the right kidney on a 3T system. The renal pyramids show lower signal intensity than the surrounding parenchyma because of the radial orientation of the tubules in the pyramids, restricting the Brownian motion of the water molecules to one direction

Conclusion

The role of MRI in renal imaging is still mainly in differentiating benign lesions versus malignant lesions in patients who cannot undergo CT scanning with intravenous iodinated contrast media, or in cases with nondiagnostic CT results. MRI and CT show comparable accuracy in detection and characterization of most renal lesions. MRI can have additional diagnostic value in the evaluation of lesions with minimal amounts of fat or with intracellular fat. Data suggest that MRI has a higher sensitivity in evaluating complicated cysts, however, the clinical implications still have to be studied. There is evidence to suggest that MRI has a higher accuracy than CT in the evaluation of early lymph node spread. MRI is a suitable tool in the preoperative work-up of potential kidney donors. Functional MRI of the kidney has not yet found broad clinical application, but it has great potential. Through the ongoing development of functional MRI techniques, we may expect an increasing role for functional MRI in the management of patients with renal disease.

References

1. Huang AJ, Lee VS, Rusinek H (2004) Functional renal MR imaging. Magn Reson Imaging Clin N Am 12:469–486
2. Martirosian P, Klose U, Mader I, Schick F (2004) FAIR true-FISP perfusion imaging of the kidneys. Magn Reson Med 51:353–361
3. Niendorf ER, Grist TM, Lee FT Jr, Brazy PC, Santyr GE (1998) Rapid in vivo measurement of single-kidney extraction fraction and glomerular filtration rate with MR imaging. Radiology 206:791–798
4. Hackstein N, Kooijman H, Tomaselli S, Rau WS (2005) Glomerular filtration rate measured using the Patlak plot technique and contrast-enhanced dynamic MRI with different amounts of gadolinium-DTPA. J Magn Reson Imaging 22:406–414
5. Pedersen M, Dissing TH, Morkenborg J et al (2005) Validation of quantitative BOLD MRI measurements in kidney: application to unilateral ureteral obstruction. Kidney Int 67:2305–2312
6. Zhang H, Prince MR (2004) Renal MR angiography. Magn Reson Imaging Clin N Am 12:487–503
7. Boss A, Martirosian P, Graf H, Claussen CD, Schlemmer HP, Schick F (2005) High resolution MR perfusion imaging of the kidneys at 3 Tesla without administration of contrast media. Rofo 177:1625–1630
8. Fukatsu H (2003) 3T MR for clinical use: update. Magn Reson Med Sci 2:37–45
9. El-Galley R (2003) Surgical management of renal tumors. Radiol Clin North Am 41:1053–1065
10. Duchene DA, Lotan Y, Cadeddu JA, Sagalowsky AI, Koeneman KS (2003) Histopathology of surgically managed renal tumors: analysis of a contemporary series. Urology 62:827–830
11. Israel GM, Bosniak MA (2003) Calcification in cystic renal masses: is it important in diagnosis? Radiology 226:47–52
12. Israel GM, Hindman N, Bosniak MA (2004) Evaluation of cystic renal masses: comparison of CT and MR imaging by using the Bosniak classification system. Radiology 231:365–371
13. Birnbaum BA, Maki DD, Chakraborty DP, Jacobs JE, Babb JS (2002) Renal cyst pseudoenhancement: evaluation with an anthropomorphic body CT phantom. Radiology 225:83–90
14. Ho VB, Choyke PL (2004) MR evaluation of solid renal masses. Magn Reson Imaging Clin N Am 12:413–427
15. Scialpi M, Di Maggio A, Midiri M, Loperfido A, Angelelli G, Rotondo A (2000) Small renal masses: assessment of lesion characterization and vascularity on dynamic contrast-enhanced MR imaging with fat suppression. AJR Am J Roentgenol 175:751–757
16. Israel GM, Bosniak MA (2005) How I do it: evaluating renal masses. Radiology 236:441–450
17. Ho VB, Allen SF, Hood MN, Choyke PL (2002) Renal masses: quantitative assessment of enhancement with dynamic MR imaging. Radiology 224:695–700
18. Patard JJ, Leray E, Rioux-Leclercq N et al (2005) Prognostic value of histologic subtypes in renal cell carcinoma: a multicenter experience. J Clin Oncol 23:2763–2771
19. Herts BR, Coll DM, Novick AC et al (2002) Enhancement characteristics of papillary renal neoplasms revealed on triphasic helical CT of the kidneys. AJR Am J Roentgenol 178:367–372
20. Pickhardt PJ, Siegel CL, McLarney JK (2001) Collecting duct carcinoma of the kidney: are imaging findings suggestive of the diagnosis? AJR Am J Roentgenol 176:627–633
21. Outwater EK, Bhatia M, Siegelman ES, Burke MA, Mitchell DG (1997) Lipid in renal clear cell carcinoma: detection on opposed-phase gradient-echo MR images. Radiology 205:103–107
22. Strotzer M, Lehner KB, Becker K (1993) Detection of fat in a renal cell carcinoma mimicking angiomyolipoma. Radiology 188:427–428
23. Henderson RJ, Germany R, Peavy PW, Eastham JA, Venable DD (1997) Fat density in renal cell carcinoma: demonstration with computerized tomography. J Urol 157:1347–1348
24. Helenon O, Chretien Y, Paraf F, Melki P, Denys A, Moreau JF (1993) Renal cell carcinoma containing fat: demonstration with CT. Radiology 188:429–430
25. Schuster TG, Ferguson MR, Baker DE, Schaldenbrand JD, Solomon MH (2004) Papillary renal cell carcinoma containing fat without calcification mimicking angiomyolipoma on CT. AJR Am J Roentgenol 183:1402–1404
26. Hammadeh MY, Thomas K, Philp T, Singh M (1998) Renal cell carcinoma containing fat mimicking angiomyolipoma: demonstration with CT scan and histopathology. Eur Radiol 8:228–229
27. D'Angelo PC, Gash JR, Horn AW, Klein FA (2002) Fat in renal cell carcinoma that lacks associated calcifications. AJR Am J Roentgenol 178:931–932
28. Kennelly MJ, Grossman HB, Cho KJ (1994) Outcome analysis of 42 cases of renal angiomyolipoma. J Urol 152:1988–1991
29. Israel GM, Bosniak MA (2005) An update of the Bosniak renal cyst classification system. Urology 66:484–488
30. Robson CJ, Churchill BM, Anderson W (1969) The results of radical nephrectomy for renal cell carcinoma. J Urol 101:297–301
31. Greene FL, Page DL, Fleming ID et al (2002) AJCC cancer staging manual. Springer, Berlin
32. Hallscheidt PJ, Bock M, Riedasch G et al (2004) Diagnostic accuracy of staging renal cell carcinomas using multidetector-row computed tomography and magnetic resonance imaging: a prospective study with histopathologic correlation. J Comput Assist Tomogr 28:333–339
33. Aslam Sohaib SA, Teh J, Nargund VH, Lumley JS, Hendry WF, Reznek RH (2002) Assessment of tumor invasion of the vena caval wall in renal cell carcinoma cases by magnetic resonance imaging. J Urol 167:1271–1275
34. Laissy JP, Menegazzo D, Debray MP et al (2000) Renal carcinoma: diagnosis of venous invasion with Gd-enhanced MR venography. Eur Radiol 10:1138–1143
35. Hallscheidt PJ, Fink C, Haferkamp A et al (2005) Preoperative staging of renal cell carcinoma with inferior vena cava thrombus using multidetector CT and MRI: prospective study with histopathological correlation. J Comput Assist Tomogr 29:64–68
36. Lawrentschuk N, Gani J, Riordan R, Esler S, Bolton DM (2005) Multidetector computed tomography vs magnetic resonance imaging for defining the upper limit of tumour thrombus in renal cell carcinoma: a study and review. BJU Int 96:291–295
37. Will O, Purkayastha S, Chan C et al (2006) Diagnostic precision of nanoparticle-enhanced MRI for lymph-node metastases: a meta-analysis. Lancet Oncol 7:52–60
38. Roy C Sr, El Ghali S, Buy X et al (2005) Significance of the pseudocapsule on MRI of renal neoplasms and its potential application for local staging: a retrospective study. AJR Am J Roentgenol 184:113–120
39. Herr HW (1999) Partial nephrectomy for unilateral renal carcinoma and a normal contralateral kidney: 10-year followup. J Urol 161:33–34; discussion 34–35

40. Pretorius ES, Siegelman ES, Ramchandani P, Cangiano T, Banner MP (1999) Renal neoplasms amenable to partial nephrectomy: MR imaging. Radiology 212:28–34
41. Yamashita Y, Honda S, Nishiharu T, Urata J, Takahashi M (1996) Detection of pseudocapsule of renal cell carcinoma with MR imaging and CT. AJR Am J Roentgenol 166:1151–1155
42. Takahashi S, Ueda J, Furukawa T et al (1996) Renal cell carcinoma: preoperative assessment for enucleative surgery with angiography, CT, and MRI. J Comput Assist Tomogr 20:863–870
43. Chahal R, Taylor K, Eardley I, Lloyd SN, Spencer JA (2005) Patients at high risk for upper tract urothelial cancer: evaluation of hydronephrosis using high resolution magnetic resonance urography. J Urol 174:478–482; quiz 801
44. Renken NS, Krestin GP (2005) Magnetic resonance imaging of the kidney. Semin Ultrasound CT MR 26:153–161
45. Kondo T, Nakazawa H, Sakai F et al (2004) Spoke-wheel-like enhancement as an important imaging finding of chromophobe cell renal carcinoma: a retrospective analysis on computed tomography and magnetic resonance imaging studies. Int J Urol 11:817–824
46. Israel GM, Hindman N, Hecht E, Krinsky G (2005) The use of opposed-phase chemical shift MRI in the diagnosis of renal angiomyolipomas. AJR Am J Roentgenol 184:1868–1872
47. Kim JK, Park SY, Shon JH, Cho KS (2004) Angiomyolipoma with minimal fat: differentiation from renal cell carcinoma at biphasic helical CT. Radiology 230:677–684
48. Roy C, Sauer B, Lindner V, Lang H, Saussine C, Jacqmin D (2007) MR imaging of papillary renal neoplasms: potential application for characterization of small renal masses. Eur Radiol 17(1):193–200
49. Verswijvel G, Vandecaveye V, Gelin G et al (2002) Diffusion-weighted MR imaging in the evaluation of renal infection: preliminary results. BJR Br J Radiol 85:100–103
50. Cakmakci H, Tasdelen N, Obuz F, Yilmaz E, Kovanlikaya A (2002) Pediatric focal xanthogranulomatous pyelonephritis: dynamic contrast-enhanced MRI findings. Clin Imaging 26:183–186
51. Kawashima A, Glockner JF, King BF Jr (2003) CT urography and MR urography. Radiol Clin North Am 41:945–961
52. Hagspiel KD, Butty S, Nandalur KR et al (2005) Magnetic resonance urography for the assessment of potential renal donors: comparison of the RARE technique with a low-dose gadolinium-enhanced magnetic resonance urography technique in the absence of pharmacological and mechanical intervention. Eur Radiol 15:2230–2237
53. Nolte-Ernsting CC, Tacke J, Adam GB et al (2001) Diuretic-enhanced gadolinium excretory MR urography: comparison of conventional gradient-echo sequences and echo-planar imaging. Eur Radiol 11:18–27
54. Regan F, Kuszyk B, Bohlman ME, Jackman S (2005) Acute ureteric calculus obstruction: unenhanced spiral CT versus HASTE MR urography and abdominal radiograph. Br J Radiol 78:506–511
55. Sudah M, Vanninen R, Partanen K, Heino A, Vainio P, Ala-Opas M (2001) MR urography in evaluation of acute flank pain: T2-weighted sequences and gadolinium-enhanced three-dimensional FLASH compared with urography. Fast low-angle shot. AJR Am J Roentgenol 176:105–112
56. Hussain SM, Kock MC, IJzermans JN, Pattynama PM, Hunink MG, Krestin GP (2003) MR imaging: a "one-stop shop" modality for preoperative evaluation of potential living kidney donors. Radiographics 23:505–520
57. Loubeyre P, Trolliet P, Cahen R, Grozel F, Labeeuw M, Minh VA (1996) MR angiography of renal artery stenosis: value of the combination of three-dimensional time-of-flight and three-dimensional phase-contrast MR angiography sequences. AJR Am J Roentgenol 167:489–494
58. Silverman JM, Friedman ML, Van Allan RJ (1996) Detection of main renal artery stenosis using phase-contrast cine MR angiography. AJR Am J Roentgenol 166:1131–1137
59. Bock M, Schoenberg SO, Schad LR, Knopp MV, Essig M, van Kaick G (1998) Interleaved gradient echo planar (IGEPI) and phase contrast CINE-PC flow measurements in the renal artery. J Magn Reson Imaging 8:889–895
60. Kock MC, IJzermans JN, Visser K et al (2005) Contrast-enhanced MR angiography and digital subtraction angiography in living renal donors: diagnostic agreement, impact on decision making, and costs. AJR Am J Roentgenol 185:448–456
61. Halpern EJ, Mitchell DG, Wechsler RJ, Outwater EK, Moritz MJ, Wilson GA (2000) Preoperative evaluation of living renal donors: comparison of CT angiography and MR angiography. Radiology 216:434–439
62. Tan SP, Bux SI, Kumar G et al (2004) Evaluation of live renal donors with three-dimensional contrast-enhanced magnetic resonance angiography in comparison to catheter angiography. Transplant Proc 36:1914–1916
63. Rankin SC, Jan W, Koffman CG (2001) Noninvasive imaging of living related kidney donors: evaluation with CT angiography and gadolinium-enhanced MR angiography. AJR Am J Roentgenol 177:349–355
64. Bhatti AA, Chugtai A, Haslam P, Talbot D, Rix DA, Soomro NA (2005) Prospective study comparing three-dimensional computed tomography and magnetic resonance imaging for evaluating the renal vascular anatomy in potential living renal donors. BJU Int 96:1105–1108
65. Hodgson DJ, Jan W, Rankin S, Koffman G, Khan MS (2006) Magnetic resonance renal angiography and venography: an analysis of 111 consecutive scans before donor nephrectomy. BJU Int 97:584–586
66. Huang AJ, Lee VS, Rusinek H (2003) MR imaging of renal function. Radiol Clin North Am 41:1001–1017
67. Vallee JP, Lazeyras F, Khan HG, Terrier F (2000) Absolute renal blood flow quantification by dynamic MRI and Gd-DTPA. Eur Radiol 10:1245–1252
68. Prasad PV, Cannillo J, Chavez DR et al (1999) First-pass renal perfusion imaging using MS-325, an albumin-targeted MRI contrast agent. Invest Radiol 34:566–571
69. Knesplova L, Krestin GP (1998) Magnetic resonance in the assessment of renal function. Eur Radiol 8:201–211
70. Fukuda Y, Ohashi I, Hanafusa K et al (2000) Anisotropic diffusion in kidney: apparent diffusion coefficient measurements for clinical use. J Magn Reson Imaging 11:156–160
71. Cova M, Squillaci E, Stacul F et al (2004) Diffusion-weighted MRI in the evaluation of renal lesions: preliminary results. Br J Radiol 77:851–857
72. Thoeny HC, De Keyzer F, Oyen RH, Peeters RR (2005) Diffusion-weighted MR imaging of kidneys in healthy volunteers and patients with parenchymal diseases: initial experience. Radiology 235:911–917
73. Chan JH, Tsui EY, Luk SH et al (2001) MR diffusion-weighted imaging of kidney: differentiation between hydronephrosis and pyonephrosis. Clin Imaging 25:110–113